











Relativistic Spin Precession in the Binary PSR J1141–6545

V. Venkatraman Krishnan^{1,2,3} , M. Bailes^{1,2,4} , W. van Straten⁵ , E. F. Keane^{1,6} , M. Kramer^{3,4} , N. D. R. Bhat^{2,7} ,
C. Flynn^{1,2} , and S. Osłowski¹ 

¹ Centre for Astrophysics and Supercomputing, Swinburne University of Technology, H11, P.O. Box 218, VIC 3122, Australia; vivekvenkris@gmail.com, vkrishnan@swin.edu.au

² ARC Centre of Excellence for All-sky Astrophysics (CAASTRO), Sydney, Australia

³ Max-Planck-Institut für Radioastronomie, Auf dem Hügel 69, D-53121 Bonn, Germany

⁴ ARC Centre of Excellence for Gravitational Wave Discovery (OzGrav), Swinburne University of Technology, Mail H11, PO Box 218, VIC 3122, Australia

⁵ Institute for Radio Astronomy and Space Research, Auckland University of Technology, New Zealand

⁶ SKA Organisation, Jodrell Bank Observatory, SK11 9DL, UK

⁷ International Centre for Radio Astronomy Research, Curtin University, Bentley, WA 6102, Australia

Received 2018 July 13; revised 2019 February 6; accepted 2019 February 23; published 2019 March 11

Abstract

PSR J1141–6545 is a precessing binary pulsar that has the rare potential to reveal the two-dimensional structure of a non-recycled pulsar emission cone. It has undergone $\sim 25^\circ$ of relativistic spin precession in the ~ 18 yr since its discovery. In this Letter, we present a detailed Bayesian analysis of the precessional evolution of the width of the total intensity profile, in order to understand the changes to the line-of-sight (LOS) impact angle (β) of the pulsar using four different physically motivated prior distribution models. Although we cannot statistically differentiate between the models with confidence, the temporal evolution of the linear and circular polarizations strongly argue that our LOS crossed the magnetic pole around MJD 54,000 and that only two models remain viable. For both of these models, it appears likely that the pulsar will precess out of our LOS in the next 3–5 yr, assuming a simple beam geometry. Marginalizing over β suggests that the pulsar is a near-orthogonal rotator and provides the first polarization-independent estimate of the scale factor (\mathbb{A}) that relates the pulsar beam opening angle (ρ) to its rotational period (P) as $\rho = \mathbb{A}P^{-0.5}$: we find it to be $>6^\circ \text{ s}^{0.5}$ at 1.4 GHz with 99% confidence. If all pulsars emit from opposite poles of a dipolar magnetic field with comparable brightness, we might expect to see evidence of an interpulse arising in PSR J1141–6545, unless the emission is patchy.

Key words: pulsars: individual (PSR J1141-6545) – radiation mechanisms: non-thermal – relativistic processes – stars: neutron

1. Introduction

Binary pulsars with short orbital periods exhibit a wide range of relativistic phenomena (Damour & Taylor 1992). These manifest themselves in, for instance, the rate of advance of periastron ($\dot{\omega}$), the amplitude of time dilation (γ), the time derivative of the orbital period (\dot{P}_b), and the range (r) and shape (s) of the Shapiro delay. Such effects are usually detected through pulsar timing, a technique where one measures the spin, Keplerian, and relativistic dynamics of the pulsar by monitoring the times of arrivals of its pulses. The measured relativistic dynamics are usually phenomenologically described by the so-called “post-Keplerian formalism” (Damour & Deruelle 1985, 1986), using such predictions of theories of gravity as the general theory of relativity (GR) that may be investigated for consistency. In systems where the spin axis of the pulsar is misaligned with the orbital angular momentum, yet another effect can be potentially observed. Named “geodetic” or “de-Sitter” precession, this is a relativistic spin–orbit coupling effect where the spin axes of the component stars of a binary system precess around the vector sum of the orbital and spin angular momenta (Damour & Ruffini 1974; Barker & O’Connell 1975; Damour & Taylor 1992). The angular rate of such precession (in rad s^{-1}) within GR is given by

$$\Omega_{\text{geod}} = n^{5/3} T_\odot^{2/3} m_c \frac{(4m_p + 3m_c)}{2(m_p + m_c)^{4/3}} \frac{1}{1 - e^2} \quad (1)$$

where $n = 2\pi/P_b$ is the angular velocity of the orbit with period P_b in seconds, $T_\odot = GM_\odot/c^3 = 4.925490947 \mu\text{s}$, m_p , and m_c are the masses of the pulsar and the companion,

respectively, in units of solar masses (M_\odot), and e is the orbital eccentricity (Lorimer & Kramer 2005). Relativistic spin precession changes the viewing angle of the pulsar beam from the Earth, causing secular variations in the observed pulse profile. Such variations have been seen in several relativistic pulsars in the past including the Hulse–Taylor pulsar PSR B1913+16 (Kramer 1998), PSR B1534+12 (Stairs et al. 2004; Fonseca et al. 2014), the double pulsar PSR J0737–3039B (Burgay et al. 2005; Breton et al. 2008), PSR J1906+0746 (Desvignes et al. 2013), and PSR J1141–6545 (Hotan et al. 2005; Manchester et al. 2010).

PSR J1141–6545 (hereafter “the pulsar”) is a young, relativistic binary pulsar in a ~ 4.74 hr eccentric ($e \sim 0.17$) orbit around a massive ($\sim 1 M_\odot$) white-dwarf companion. It was discovered in 2000 in the Parkes Multibeam Pulsar Survey (Kaspi et al. 2000) and regular pulsar timing observations have been carried out since then. Given the compact configuration of the binary system, $\dot{\omega}$, γ , and \dot{P}_b were soon measured, leading to a test of GR with $\sim 25\%$ precision (Bailes et al. 2003). Bhat et al. (2008) performed a $\sim 6\%$ test of GR along with the estimates of the inclination angle of the system to be $\sim 71^\circ$, whose equally likely degenerate solution of $\sim 109^\circ$ is now ruled out by a recent study of the annual variations of the pulsar’s scintillation velocity (Reardon et al. 2019). The GR masses of the pulsar and the companion were obtained through pulsar timing, providing an estimate of geodetic precession rate of the pulsar of 1.36 yr^{-1} , implying a precession period of ~ 265 yr (Hotan et al. 2005; hereafter H05). As such a precession rate

profile at 10% of the peak pulsed flux density. Hence, our estimates of the width have bigger uncertainties. We perform the estimation using the TRANSITIONS pulse width estimation algorithm of the PSRSTAT program in PSRCHIVE.⁹ Following Maciesiak et al. (2011), we multiply this estimate by 1.1 to obtain the pulse width at the 1% signal-to-noise level, which we assume to be the width of the emitted pulse. We use the polarization information to understand and distinguish between several width evolution models as we describe below.

2.1.1. Width Evolution Models

Assuming a circularly symmetric cone of radio emission from the pulsar, one can geometrically relate the instantaneous pulse widths (W) to the opening angle of the emission cone (ρ) as

$$\cos \rho = \cos \alpha \cos \zeta + \sin \alpha \sin \zeta \cos(W/2) \quad (5)$$

(Gil et al. 1984). For non-recycled pulsars, ρ is generally consistent with the relation

$$\rho = \mathbb{A} P_{\text{spin}}^{-0.5}, \quad (6)$$

where P_{spin} is the spin period of the pulsar and \mathbb{A} is a constant of proportionality (hereafter the ‘‘scale factor’’; Lorimer & Kramer 2005). Several empirical estimates of \mathbb{A} have been made with an ensemble of pulsars with their angles (α , λ) estimated from the RVM (see Maciesiak et al. 2011 and references therein). With P_{spin} measured in seconds, and ρ measured in degrees, the value of \mathbb{A} at 1.4 GHz is estimated to lie in the range $4.9 \text{ s}^{0.5} - 6.5 \text{ s}^{0.5}$ (e.g.: Biggs 1990; Rankin 1990; Kramer et al. 1994; Gil & Han 1996; Maciesiak et al. 2011). The temporal variations in ρ and α are negligible for the timescale of our data set, so the evolution of W is expected to track β .

We performed Markov Chain Monte Carlo (MCMC) fits of Equation (5) to our data. First, we used a meanshift clustering algorithm to group observations that are closely spaced in time, resulting in ~ 34 ‘‘clusters’’ (C_i), each of which is assigned one model parameter β_i to denote the impact angle at that time. We then added one global model parameter each for α and \mathbb{A} for a total of 36 parameters. We set uniform priors for α between 0° and 180° ¹⁰ and \mathbb{A} between $4^\circ \text{ s}^{0.5}$ and $8^\circ \text{ s}^{0.5}$ with the rationale that uniform priors are non-informative, and offer no biases to our posterior estimates.

Our initial model fits with the prior on all β_i as $U(-\rho, \rho)$ resulted in axisymmetric, bi-modal posterior probability distributions for β_i . The two modes of the posterior distributions were non-overlapping for most of the data set, except for when $\beta_i \rightarrow 0$, where the distinct modes merged into a single distribution. To remain agnostic about the sign of β_i , we used four different prior models ($M_k^{\text{prior}} \forall k = \{1, 2, 3, 4\}$), each with different priors on β_i (see Table 1), thereby breaking the bi-modal posterior degeneracy on β_i for every M_k^{prior} . The extrema across all the models were chosen to be between $-\rho$ and ρ , as $|\beta| < \rho$ is necessary for pulse detection. The models

M_1^{prior} and M_2^{prior} assume that the signs of β_i stay negative and positive, respectively, for the entire data set, while M_3^{prior} and M_4^{prior} assume there is a sign flip at MJD 54,000. To make sure that the uncertainties on β_i are estimated correctly for cases where $\beta_i \rightarrow 0$, an additional $\pm 1^\circ$ was added to the prior limits whose extremum was otherwise zero. This 1° was chosen based on the fact that the average 99% confidence interval on the estimate of β_i was $< 1^\circ$. The choice of MJD = 54,000 as the pivotal cluster point that distinguishes the models was motivated by three reasons. First, M10’s analysis points to a minimum value of $|\beta_i|$ around this MJD. Second, the first indication of a sign flip in the circular polarization profile also happens around this MJD (see Figure 4). Third, the pulsar experienced a rotational glitch soon after this MJD (at MJD $\sim 54,272$).

For every M_k^{prior} , we marginalize over \mathbb{A} to infer the values of $\{\alpha, \beta_i\}$. We used the Gelman–Rubin criterion to assess the convergence of our MCMC chains and used maximum likelihood statistics to compute the parameter uncertainties given the asymmetric posterior distributions (using the CHAINCONSUMER package; Hinton 2016). For each of our MCMC point (P_j), we obtain λ_i from α and β_i . With this, we perform another MCMC fit to estimate the angles ϕ_0 and δ using the relations

$$\cos \lambda = \cos i \cos \delta - \sin \delta \sin i \cos \phi, \quad (7)$$

$$\phi = \phi_0 + \Omega_{\text{geod}}(t - t_0), \quad (8)$$

where ϕ_0 is the reference precession phase at time $t = t_0$ (Damour & Taylor 1992); where t_0 is set to MJD 52,905. For every MCMC point in the second run (Q_k), we iterate over each of P_j , and compute the χ^2 of fitting the function given by Equations (7) and (8) with the values (ϕ_0, δ) from Q_k to λ_i from P_j . The likelihood of Q_k is then defined as the sum of the χ^2 over all P_j . Here we use the inclination angle value of 71° obtained from pulsar timing (Bhat et al. 2008) and use the GR value for Ω_{geod} obtained from Equation (1).

3. Results and Discussion

The posterior distributions of $\{\alpha, \mathbb{A}\} \forall M_k^{\text{prior}}$ after marginalizing over β_i are shown in Figure 2 and their 68% confidence limits are presented in Table 1. This analysis provides the first self-consistent estimate of \mathbb{A} independent of the pulsar’s polarization profile. As seen in Figure 2, despite being asymmetric with a leading tail, the posterior distribution of \mathbb{A} is confined to be $> 6^\circ \text{ s}^{0.5}$ with 99% confidence.

Marginalizing over M_k^{prior} and \mathbb{A} suggests that the pulsar is a nearly orthogonal rotator with $\alpha = 89^{+18}_{-17}$ at 68% confidence. Such an orientation, combined with 7° to 14° of precession of β , could have resulted in the detection of the pulsar’s interpulse. However, an interpulse has not been observed in our data set. Given the narrow duty cycle of the pulsar, if one assumes the Double Pole—InterPulse (DP-IP) model of (the lack of) interpulse emission (Lorimer & Kramer 2005), then a further constraint can be added on the posterior distribution of α so that

$$2\alpha < \pi - (\beta + \rho). \quad (9)$$

This constraint rules out the entire 68% confidence interval on α for every M_k^{prior} . Another possibility is that the other pole’s emission is fainter than our detection threshold. If so, future

⁹ <http://psrchive.sourceforge.net/manuals/psrstat/algorithms/width>

¹⁰ We note that there have been a number of probability distributions discussed in the literature for α (e.g., Gil & Han 1996; Zhang et al. 2003). However, we think it is best to provide here the most conservative estimate of α with a non-informative prior. We also report that changing the prior to the naturally expected distribution of $\sin(\alpha)$ provides posterior distributions that are consistent with what is presented here.

Table 1
Model Priors for β_i with Corresponding Relative Bayesian Information Criterion Values and Posteriors for α and \mathbb{A} with 68% Confidence Intervals

Model	Prior on β_i	α (degrees)	\mathbb{A}	ΔBIC	δ (degrees)	ϕ_0 (degrees)
M_1^{prior}	$U(-\rho, 1)$	90_{-9}^{+12}	$6.53_{-0.10}^{+0.06}$	0.0	38 ± 13 and 155 ± 20	226 ± 36 and 314 ± 24
M_2^{prior}	$U(1, \rho)$	84_{-6}^{+13}	$6.54_{-0.10}^{+0.03}$	0.3	35 ± 21 and 149 ± 21	33 ± 36 and 132 ± 44
M_3^{prior}	$U(-\rho, 1)$ MJD ≤ 54000 $U(-1, \rho)$ otherwise	88_{-10}^{+9}	$6.54_{-0.10}^{+0.04}$	0.1	91 ± 60	81 ± 39
M_4^{prior}	$U(-1, \rho)$ MJD ≤ 54000 $U(-\rho, 1)$ otherwise	93_{-9}^{+9}	$6.54_{-0.10}^{+0.05}$	0.5	60 ± 24 and 126 ± 24	273 ± 35

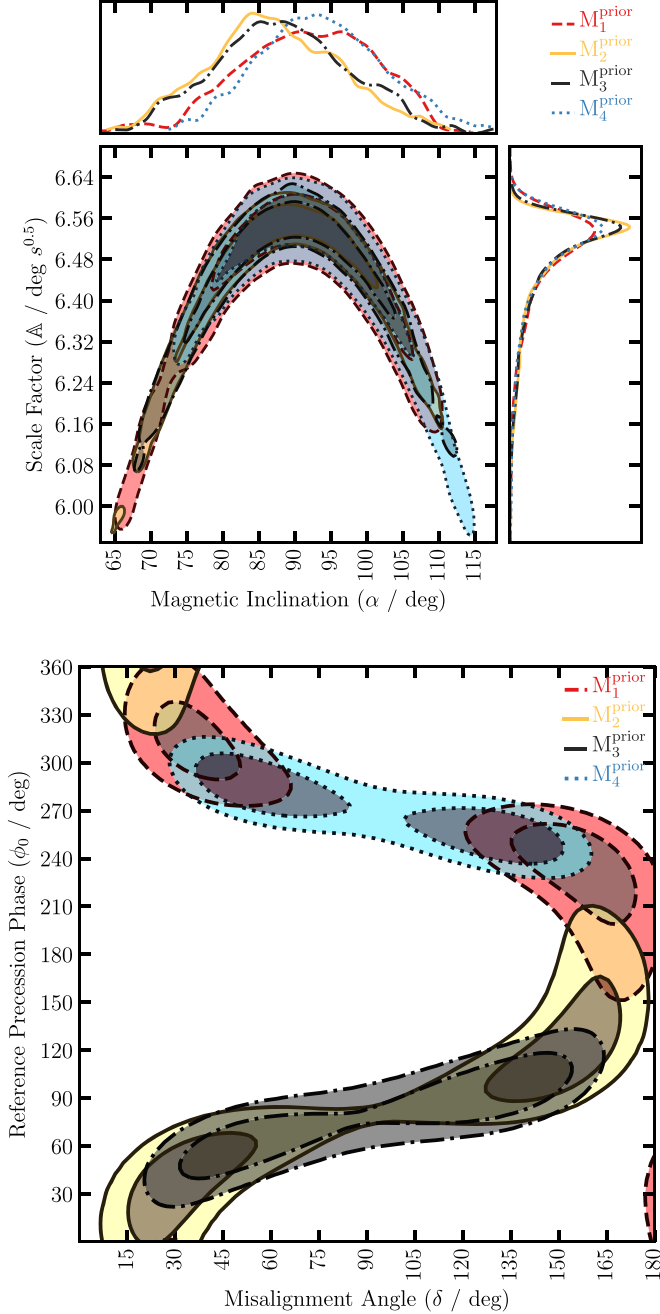


Figure 2. Top: the 68% and 95% contour confidence intervals of the magnetic inclination angle (α) and the scale factor (\mathbb{A}) along with their marginalized posterior distributions for all M_k^{prior} . Bottom: the corresponding contours of the spin-misalignment angle (δ) and the reference precession phase (ϕ_0).

observations with the new Parkes Ultra Wideband Low (UWL) receiver (Dunning et al. 2015) and the MeerKAT telescopes (Bailes et al. 2018), with their much improved sensitivity and frequency coverage, might be able to detect such an interpulse, which will confirm our estimates of α . Yet another possibility is that our initial assumption of a circularly symmetric emission cone is simplistic. Alternative beam shapes such as fan beam models (Dyks et al. 2010; Wang et al. 2014) have been proposed to explain the complex structures generally seen in the pulse profiles of other pulsars. Investigating such alternate beam shapes is beyond the scope of this Letter.

Our results are in striking contrast with the 1σ estimates of $\alpha = 160_{-16}^{+8}$ obtained by M10 using the PA profile. For conventional models, such a value seems unphysical for a number of reasons. First, assuming M10’s value of α , one can compute the expected pulse width for every β_i . Even with a conservative marginalization over just the unbiased uniform prior probability distribution of \mathbb{A} between 4.9 and $6.5 \text{ s}^{0.5}$, the change of the pulse widths for this α is expected to be between $\sim 15^\circ$ and $\sim 41^\circ$, regardless of the sign of evolution of β_i . However, as seen in Figure 3, the observed evolution of the pulse width is only between $\sim 5^\circ$ and $\sim 16^\circ$. For such values of α to match the observed pulse widths, the value of \mathbb{A} must be tuned to ~ 4 . Such a value of \mathbb{A} has not been seen in any young pulsar, assuming circularly symmetric beaming. Second, M10 suggested that the evolution of β reached its maximum value $\beta_{\text{max}} \sim -1^\circ$ near MJD 54,000. This prompted them to suggest that there would be a “reversal” of shape variations into the next decade as the observer’s LOS retraces its path. However, as seen in Figures 3 and 4 the evolution of width and polarization of the pulse profile are not at all symmetric in our significantly longer data set.

Such inconsistencies are possibly due to the pulsar’s complicated PA profile deviating from an ideal RVM sweep. First, the central part of the polarization profile appears to evolve with frequency, part of which is seen to be absorbed into RM estimates leading to unphysical pulse-phase dependent, secular variations of inferred RM. M10 fit for the RVM over just the wings of the profile. However, the center of the profile can be crucial for values of β close to 0, as $\beta \rightarrow 0 \Rightarrow \frac{d\Psi}{d\Phi} \rightarrow \infty$. Second, we see orthogonally polarized modes (OPMs; Gangadhara 1997) in the PA sweep that evolve to non-OPMs over the data set. Third, such an OPM transition, when occurring at the central part of the profile where the slope of PA is the steepest, means that it is impossible to know if a non-orthogonal step change Ψ_{step} is the observed value by itself, the value after an OPM correction ($90^\circ \pm \Psi_{\text{step}}$), or the value after a phase unwrap ($180^\circ \pm \Psi_{\text{step}}$). Such degeneracies can also affect the absolute central PA (Ψ_0) that M10 used to

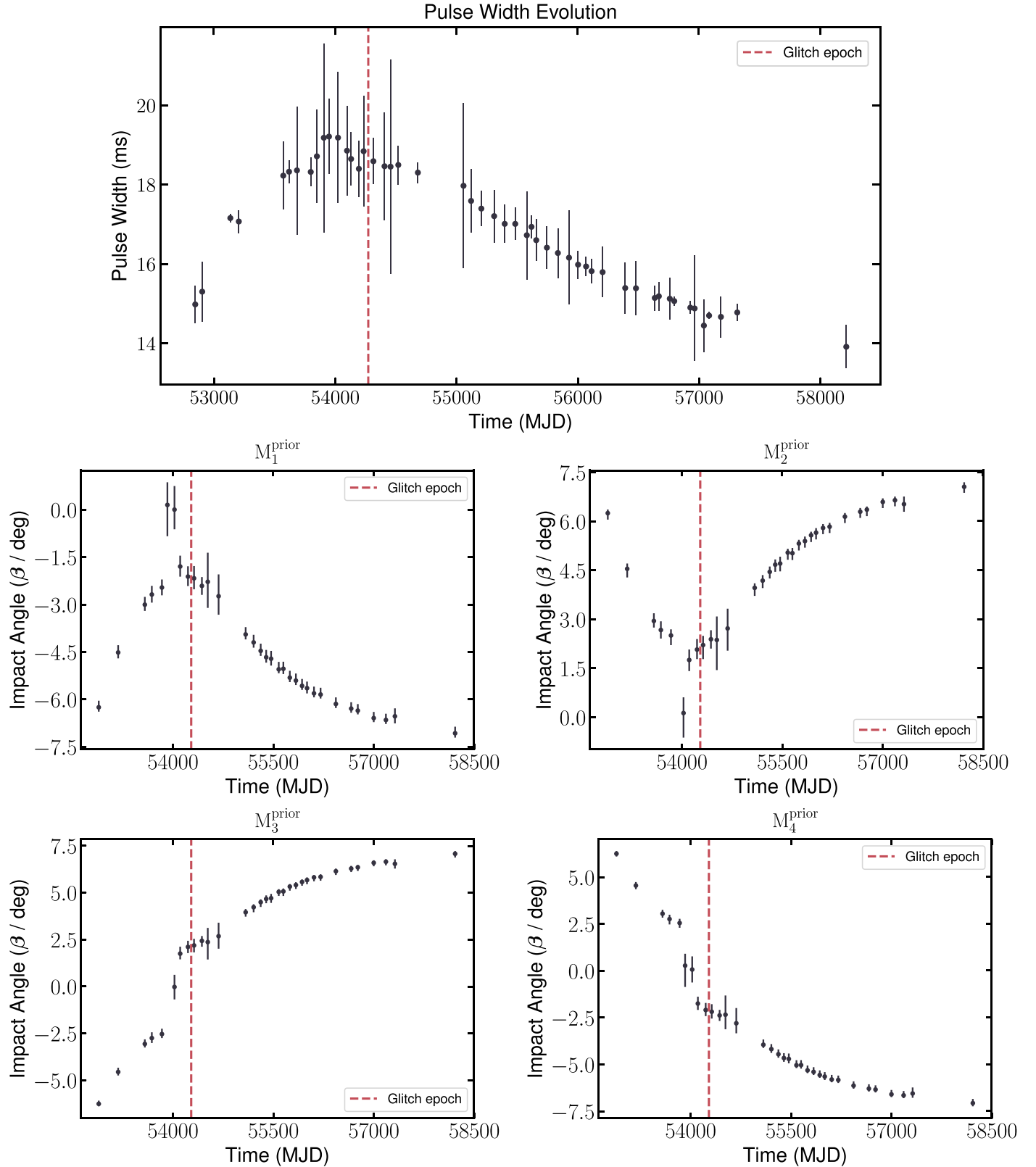


Figure 3. Top: the temporal evolution of pulse width at the 10% of the peak pulsed flux density. Remaining panels: the corresponding variations of β for the prior models $M_k^{\text{prior}} \forall k = \{1, 2, 3, 4\}$. The red dashed line in all of the plots indicates the glitch epoch. The black dots indicate the mean value, and the black lines indicate their corresponding 68% confidence intervals.

compute the longitude of precession (η). Given such complexities in the PA swing, we find the RVM to be too simplistic to be used as is for this pulsar.

Our Bayesian Information Criterion (BIC) test between the four models could not clearly distinguish the best model (see Table 1). However, there are two physical arguments that could

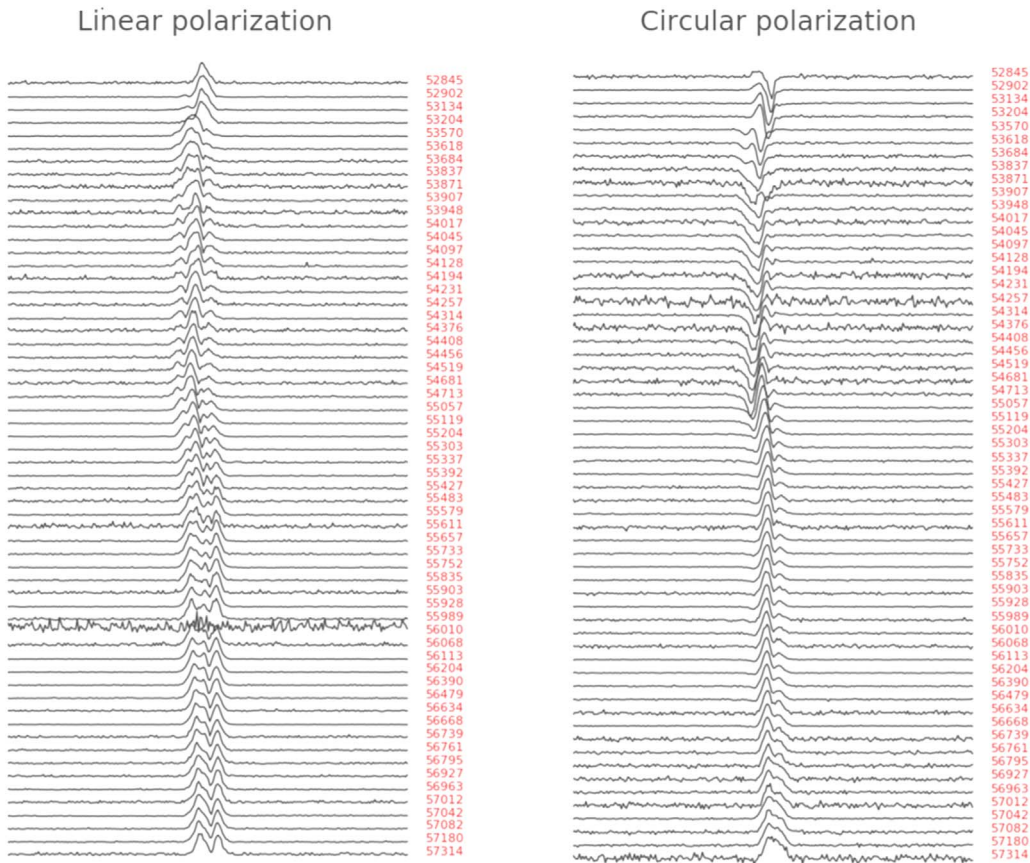


Figure 4. Temporal evolution of linear (left) and circular polarization (right) profiles of PSR J1141–6545. Each line spans 0.6 in pulse phase. The number on the right denotes the mean MJD of closely spaced observations clustered using a meanshift estimator (see the text). Each line’s amplitude is normalized to its peak. The evolution of the polarization rules out any symmetry in the shape variations about MJD $\sim 54,000$. The coincident sign flip in circular polarization suggests that the LOS may have crossed the magnetic axis of the pulsar.

be used to differentiate the models. First, most regions of the posterior distribution of ϕ_0 for M_1^{prior} and M_2^{prior} fail to predict the sharp turnover (which happens when $\phi = 0^\circ$ or 180°) in the evolution of β seen in these models, and hence those models are disfavored. Additionally, the detection of a sign flip in circular polarization around the epoch of minimum $|\beta|$ suggests that our LOS has crossed the magnetic axis during the course of our observing campaign, thereby favoring models M_3^{prior} and M_4^{prior} . This might explain the fact that we do not see a reversal of shape variations as M10 predicted. If true, regular observations of this pulsar until it precesses out of our LOS will give us the first glimpse of the two-dimensional structure of a large fraction of the pulsar emission cone. Regardless of the choice of M_k^{prior} , our analysis indicates that the pulsar will precess out of our LOS in the next 3–5 yr. The posterior distributions of ϕ_0 and δ are plotted in Figure 2 and their 68% confidence intervals are reported in Table 1. Without knowledge of the evolution of β , it is presently not possible to significantly constrain the possible values for ϕ_0 and δ . Future observations with the Parkes UWL receiver might help resolve the ambiguities in the RM of the pulsar, which can then be utilized to obtain reliable constraints of the pulsar geometry from its RVM. Comparing such constraints with the ones obtained in this Letter might provide further insights on the system’s orbital geometry.

It is also interesting that a rotational glitch takes place soon after the supposed reversal. It is possible that M10’s projections were correct but that the glitch reconfigured the pulsar’s

magnetosphere resulting in changes to the observed pulse profile. To check if the glitch had altered α , we performed a BIC test of all M_k^{prior} with two model parameters for α at either side of the glitch epoch. This returned consistent posteriors and disfavored the split of α , thus ruling out any major magnetospheric reconfiguration as a result of the glitch. However, we cannot rule out any glitch induced change in emission properties that did not change α .



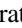
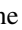



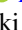
4. Conclusions

We performed an analysis of the evolving pulse widths of PSR J1141–6545 due to spin precession using ~ 18 yr of observations with robust polarization calibration and pulse width estimation methods. While we cannot uniquely infer the sign of the impact angle β for every observation, the absolute magnitude is well constrained. The circular polarization sign flip at MJD $\sim 54,000$, combined with the temporally asymmetric shape variations, supports a magnetic axis cross-over. Our estimate of the magnetic inclination angle α , regardless of M_k^{prior} , indicates that the pulsar is a near-orthogonal rotator. The absence of an observed interpulse emission motivates continued monitoring of this pulsar with more sensitive instruments like the Parkes UWL receiver and the MeerKAT telescope.

We thank the anonymous referee for a thorough cross-check of our analysis, along with numerous suggestions that have

significantly improved the manuscript. We thank N. Wex and P.C.C. Freire for useful discussions and suggestions. The Parkes radio telescope is funded by the Commonwealth of Australia for operation as a National Facility managed by CSIRO. This research was primarily supported by the Australian Research Council Centre of Excellence for All-sky Astrophysics (CAASTRO; project number CE110001020). Computations were performed on the gSTAR/ozSTAR national facilities at Swinburne University of Technology funded by Swinburne and the Australian Government's Education Investment Fund. S.O. acknowledges the Australian Research Council grant Laureate Fellowship FL150100148. N. D.R.B. acknowledges the support from a Curtin Research Fellowship (CRF12228). M.B. acknowledges the Australian Research Council grants OzGrav (CE170100004) and The Laureate fellowship (FL150100148).

ORCID iDs

V. Venkatraman Krishnan  <https://orcid.org/0000-0001-9518-9819>
M. Bailes  <https://orcid.org/0000-0003-3294-3081>
W. van Straten  <https://orcid.org/0000-0003-2519-7375>
E. F. Keane  <https://orcid.org/0000-0002-4553-655X>
M. Kramer  <https://orcid.org/0000-0002-4175-2271>
N. D. R. Bhat  <https://orcid.org/0000-0002-8383-5059>
C. Flynn  <https://orcid.org/0000-0002-4796-745X>
S. Osłowski  <https://orcid.org/0000-0003-0289-0732>

References

Bailes, M., Barr, E., Bhat, N. D. R., et al. 2018, arXiv:1803.07424
Bailes, M., Ord, S. M., Knight, H. S., & Hotan, A. W. 2003, *ApJL*, **595**, L49
Barker, B. M., & O'Connell, R. F. 1975, *PhRvD*, **12**, 329

Bhat, N. D. R., Bailes, M., & Verbiest, J. P. W. 2008, *PhRvD*, **77**, 124017
Biggs, J. D. 1990, *MNRAS*, **245**, 514
Breton, R. P., Kaspi, V. M., Kramer, M., et al. 2008, *Sci*, **321**, 104
Burgay, M., Possenti, A., Manchester, R. N., et al. 2005, *ApJL*, **624**, L113
Damour, T., & Deruelle, N. 1985, *Ann. Inst. Henri Poincaré Phys. Théor.*, **43**, 107
Damour, T., & Deruelle, N. 1986, *Ann. Inst. Henri Poincaré Phys. Théor.*, **44**, 263
Damour, T., & Ruffini, R. 1974, *CRASM*, **279**, 971
Damour, T., & Taylor, J. H. 1992, *PhRvD*, **45**, 1840
Desvignes, G., Kramer, M., Cognard, I., et al. 2013, in *IAU Symp. 291, Neutron Stars and Pulsars: Challenges and Opportunities after 80 Years*, ed. J. van Leeuwen (Cambridge: Cambridge Univ. Press), 199
Dunning, A., Bowen, M., Bourne, M., Hayman, D., & Smith, S. L. 2015, in *2015 IEEE-APS Topical Conf. Antennas and Propagation in Wireless Communications (APWC)* (Piscataway, NJ: IEEE), 787
Dyks, J., Rudak, B., & Demorest, P. 2010, *MNRAS*, **401**, 1781
Fonseca, E., Stairs, I. H., & Thorsett, S. E. 2014, *ApJ*, **787**, 82
Gangadhara, R. T. 1997, *A&A*, **327**, 155
Gil, J., Gronkowski, P., & Rudnicki, W. 1984, *A&A*, **132**, 312
Gil, J. A., & Han, J. L. 1996, *ApJ*, **458**, 265
Hinton, S. R. 2016, *JOSS*, **1**, 00045
Hotan, A. W., Bailes, M., & Ord, S. M. 2005, *ApJ*, **624**, 906
Kaspi, V. M., Lyne, A. G., Manchester, R. N., et al. 2000, *ApJ*, **543**, 321
Kramer, M. 1998, *ApJ*, **509**, 856
Kramer, M., & Wex, N. 2009, *CQGra*, **26**, 073001
Kramer, M., Wielebinski, R., Jessner, A., Gil, J. A., & Seiradakis, J. H. 1994, *A&AS*, **107**, 515
Lorimer, D. R., & Kramer, M. 2005, *Handbook of Pulsar Astronomy* (New York: Cambridge Univ. Press)
Maciesiak, K., Gil, J., & Ribeiro, V. A. R. M. 2011, *MNRAS*, **414**, 1314
Manchester, R. N., Hobbs, G., Bailes, M., et al. 2013, *PASA*, **30**, e017
Manchester, R. N., Kramer, M., Stairs, I. H., et al. 2010, *ApJ*, **710**, 1694
Radhakrishnan, V., & Cooke, D. J. 1969, *ApL*, **3**, 225
Rankin, J. M. 1990, *ApJ*, **352**, 247
Reardon, D. J., Coles, W. A., Hobbs, G., et al. 2019, arXiv:1903.01990
Stairs, I. H., Thorsett, S. E., & Arzoumanian, Z. 2004, *PhRvL*, **93**, 141101
Staveley-Smith, L., Wilson, W. E., Bird, T. S., et al. 1996, *PASA*, **13**, 243
van Straten, W. 2013, *ApJS*, **204**, 13
Wang, H. G., Pi, F. P., Zheng, X. P., et al. 2014, *ApJ*, **789**, 73
Zhang, L., Jiang, Z.-J., & Mei, D.-C. 2003, *PASJ*, **55**, 461